Article

Novel Patterns in Fractional-in-Space Nonlinear Coupled FitzHugh–Nagumo Models with Riesz Fractional Derivative

Xiaoyu Li, Che Han and Yulan Wang *

College of Science, Inner Mongolia University of Technology, Hohhot 010051, China; fish_li82@163.com (X.L.); hanche0905@163.com (C.H.)
* Correspondence: wylnei@163.com; Tel.: +86-0471-657-5470

Abstract: In this paper, the Fourier spectral method is used to solve the fractional-in-space nonlinear coupled FitzHugh–Nagumo model.Numerical simulation is carried out to elucidate the diffusion behavior of patterns for the fractional 2D and 3D FitzHugh–Nagumo model. The results of numerical experiments are consistent with the theoretical results of other scholars, which verifies the accuracy of the method. We show that stable spatio-temporal patterns can be sustained for a long time; these patterns are different from any previously obtained in numerical studies. Here, we show that behavior patterns can be described well by the fractional FitzHugh–Nagumo and Gray–Scott models, which have unique properties that integer models do not have. Results show that the Fourier spectral method has strong competitiveness, reliability, and solving ability for solving 2D and 3D fractional-in-space nonlinear reaction-diffusion models.

Keywords: Riesz fractional derivative; FitzHugh–Nagumo model; spatial patterns; Fourier spectral method

1. Introduction

In the past few decades, the theory and application of fractional calculus have been widely concerned and rapidly developed because it can more accurately simulate various physical processes in nature, especially suitable for characterizing the memory and genetic properties of materials and processes. Applications of fractional calculus include control theory [1], non-Newtonian fluid dynamics [2], rheology [3], hysteretic phenomena [4], dynamical systems [5], viscoelastic theory [6], and abnormal diffusion [7–9]. Most of these problems can be expressed as fractional differential equations (FDEs), so it is of great significance to study the analytical or numerical methods of FDEs. Analytical methods for solving nonlinear FDEs have an Adomian decomposition method [10], new iteration method [11], homotopy perturbation method [12], and so on. In these methods, the solution does not require discrete equations or approximation operators. Because these methods produce local solutions under initial conditions, it is necessary to use numerical methods to study the long time properties of solutions of FDEs. Accurate and time-saving numerical methods are needed for the study of fractional-order dynamical systems and their related phenomena, such as patterns and chaos. Therefore, the development of time-saving, accurate, and stable numerical methods of FDEs is a focus. Some numerical methods of the FDEs have been announced, such as the finite difference method [13], finite difference predictor-corrector method [14,15], reproducing kernel method [16,17], matrix approach method [18], spectral method [19–22], and so on [23–29].

The Fourier spectral method [19–22,30,31] is a good method for studying the fractional diffusion model. Some scholars used the Fourier spectral method to solve the space fractional Klein–Gordon–Schrödinger equations [19], modified Swift–Hohenberg equation [20], fractional variable-coefficient KdV-modified KdV equation [30], and 2D space fractional Gray–Scott model [31], and so on [21,22]. In this manuscript, we use the Fourier spectral method for spatial discretization and the Runge–Kutta method for time discretization to

solve the FitzHugh–Nagumo model with the Riesz fractional derivative.

FitzHugh [32] proposed a mathematical model of excitable media applied to neuronal dynamics. This model is called the FitzHugh model. The early FitzHugh model was a nonlinear ordinary differential equation. Then, Nagumo [33] extended the early FitzHugh model to derive the FitzHugh–Nagumo model. The most important characteristic of the FitzHugh–Nagumo model is that the solutions of the model can be excited within a certain range of control parameters. Therefore, it is one of the best models to study excitable systems and excitable helical waves. Bueno–Orovio [21] used the Fourier spectral method and fractional Fick's law [34,35] to solve the space fractional FHN model. Liu and Zhang [36] used a semi-alternating direction method for solving a 2D fractional FHN monodomain model on an approximate irregular domain. With the development of fractional calculus, this paper considers the following space fractional 3D coupled FitzHugh–Nagumo models with Riesz fractional derivatives:

$$
\begin{cases}
\dfrac{\partial u}{\partial t} = -K_u(-\Delta^{\frac{\alpha}{2}})u - u(1-u)(u-\mu) - v, \\
\dfrac{\partial v}{\partial t} = \varepsilon(\beta u - v),
\end{cases}
\tag{1}
$$

with the initial conditions:

$$
u(x,y,z,0) = u_0(x,y,z), \quad v(x,y,z,0) = v_0(x,y,z).
\tag{2}
$$

where $(x,y,z,t) \in \Omega \times [0,T]$, $\Omega = (a,b) \times (a,b) \times (a,b)$ and $1 < \alpha \le 2$. ε, μ, β and k are constants. K_u are the diffusion coefficients. The fractional Laplacian operator with Riesz fractional derivative is defined as:

$$
-(-\Delta^{\frac{\alpha}{2}})v = \frac{\partial^\alpha v}{\partial |x|^\alpha} + \frac{\partial^\alpha v}{\partial |y|^\alpha} + \frac{\partial^\alpha v}{\partial |z|^\alpha} = -\frac{1}{2\cos \pi\alpha/2}\left({}_xD_L^\alpha v + {}_xD_R^\alpha v + {}_yD_L^\alpha v + {}_yD_R^\alpha v + {}_zD_L^\alpha v + {}_zD_R^\alpha v\right),
\tag{3}
$$

with ${}_xD_L^\alpha, {}_xD_R^\alpha, {}_yD_L^\alpha, {}_yD_R^\alpha$, and ${}_zD_L^\alpha, {}_zD_R^\alpha$ being the Riemann-Liouville fractional operators as follows [37–40]:

$$
{}_xD_L^\alpha v = \frac{1}{\Gamma(2-\alpha)}\frac{d^2}{dx^2}\left(\int_a^x (x-\tau)^{1-\alpha}v(\tau,y,z,t)d\tau\right),
\tag{4}
$$

$$
{}_xD_R^\alpha v = \frac{1}{\Gamma(2-\alpha)}\frac{d^2}{dx^2}\left(\int_x^b (\tau-x)^{1-\alpha}v(\tau,y,z,t)d\tau\right).
\tag{5}
$$

Definition 1. *The Riesz fractional derivative [27,28] of order $\alpha \in (0,1)$ is given by:*

$$
D^\alpha h(x) = \frac{d}{dx}H_x^{1-\alpha}h(x) = \frac{1}{2\Gamma(1-\alpha)\cos\frac{\pi\alpha}{2}}\frac{d}{dx}\int_{-\infty}^\infty \frac{sgn(x-\tau)}{|x-\tau|^\alpha}h(\tau)d\tau, \quad x \in R.
\tag{6}
$$

where $H_x^\alpha h(x)$ is the conjugate Riesz potential [41,42] of the order $\alpha \in (0,1)$.

Definition 2. *The conjugate Riesz potential [41,42] of the order $\alpha \in (0,1)$ takes the following form:*

$$
H_x^\alpha h(x) = \frac{1}{2\Gamma(\alpha)\sin\frac{\pi\alpha}{2}}\int_{-\infty}^\infty \frac{sgn(x-\tau)}{|x-\tau|^{1-\alpha}}h(\tau)d\tau, \quad x \in R.
\tag{7}
$$

The Fourier transforms of Riesz fractional derivative for $\alpha \in (0,1)$ is presented as:

$$
\mathcal{F}_x[D_x^\alpha h(x)](\omega) = |\omega|^\alpha \hat{h}(\omega).
\tag{8}
$$

2. Numerical Method

In order to normalize the space interval $[a,b]$ to $[0,2\pi]$, we let $x \to \frac{2\pi(x-a)}{L}, y \to \frac{2\pi(y-a)}{L}, z \to \frac{2\pi(z-a)}{L}$ and $L = b-a$, $x_i = i\Delta x = \frac{2\pi Li}{N}$, $y_i = i\Delta y = \frac{2\pi Li}{N}$, $z_i = i\Delta z = \frac{2\pi Li}{N}$,

$i = -N/2, -N/2 + 1, \cdots\cdots, N/2 - 1, N > 0$ and N is an integer.

The discrete Fourier transform(DFT) definition as:

$$\hat{h}(k_x, k_y, k_z, t) = \mathcal{F}(h) = \frac{1}{N^3} \sum_{j=-\frac{N}{2}}^{\frac{N}{2}-1} \sum_{j=-\frac{N}{2}}^{\frac{N}{2}-1} \sum_{j=-\frac{N}{2}}^{\frac{N}{2}-1} h(x_j, y_j, z_j, t) e^{-ik_x x_j - ik_y y_j - ik_z z_j}, \quad (9)$$

Using the discrete Fourier transform (9) for u, v in the spatial domain. Equation (1) can be transformed into the following ordinary differential equations (ODEs) about t.

$$\begin{cases} \frac{\partial U}{\partial t} = F(t, U), \\ U(K\alpha, 0) = U_0. \end{cases} \quad (10)$$

where:

$$\begin{aligned}
& K\alpha = |\lambda_x|^\alpha + |\lambda_y|^\alpha + |\lambda_z|^\alpha, \quad \hat{\phi} = \begin{pmatrix} \hat{u} \\ \hat{v} \end{pmatrix}, \quad r(t, \hat{\phi}) = \begin{pmatrix} \frac{\partial \hat{u}}{\partial t} \\ \frac{\partial \hat{v}}{\partial t} \end{pmatrix}, \\
& U = (\hat{\phi}_0(K\alpha, t), \hat{\phi}_1(K\alpha, t), \cdots, \hat{\phi}_{N-1}(K\alpha, t))^T, \\
& F(t, U) = (r_0(t, \hat{\phi}_0(t)), r_1(t, \hat{\phi}_0(t)), \cdots, r_{N-1}(t, \hat{\phi}_{N-1}(t)))^T, \\
& U_0(K\alpha) = (\hat{\phi}_{00}(K\alpha), \hat{\phi}_{01}(K\alpha), \cdots, \hat{\phi}_{0(N-1)}(K\alpha))^T,
\end{aligned} \quad (11)$$

Definition 3. *Fourth-order Runge–Kutta method(RKM) for ODEs (10) in the form of:*

$$U_{n+1} = U_n + \tau \eta(U_n, t_n, \tau), \quad (12)$$

where incremental function $\eta(U_n, t_n, \tau)$ is determined by $F(t, U)$.

Definition 4. *If for any differential equations $\frac{\partial U}{\partial t} = F(t, U)$ which satisfies the Lipschitz condition when $\tau = \frac{T}{n}$, $n \longrightarrow \infty$ and $U_0(K\alpha) \longrightarrow U(K\alpha, 0)$, there is $u_n \longrightarrow U(t)$ for any $0 \le t \le T$, then Equation (12) is convergent [30,31].*

Theorem 1. *If $\eta(U, t, \tau)$ satisfies the Lipschitz condition in U, then the numerical method given by Equation (12) is stable.*

Proof. We refer the reader to [30,31] for the details of the proof. □

Lemma 1. *If $\|e_{n+1}\| \le (1 + \tau L_1)\|e_n\| + c$, then Equation (12) is fourth order one-step method and the error estimate is as follows:*

$$|e_n| \le e^{L_1 T}(|e_0| + L_1 \tau e + cT\tau^4), \quad (13)$$

where $e_n = U_n - U(t_n)$ and c is constant. where L_1 is lipschitz constant and $e = max(|e_0|, |e_1|, \cdots, |e_{n-1}|)$. τ is step-size and $n = 1, \cdots, \frac{T}{\tau}$.

Proof. For the details of the proof, one may refer to [30,31]. □

Then, we use the following inverse discrete Fourier transform(IDFT) (14), and can obtain the numerical solution. The inverse discrete Fourier transform definition as:

$$h(x_j, y_j, z_j, t) = \mathcal{F}^{-1}(\hat{h}) = \sum_{k_x=-\frac{N}{2}}^{\frac{N}{2}-1} \sum_{k_y=-\frac{N}{2}}^{\frac{N}{2}-1} \sum_{k_z=-\frac{N}{2}}^{\frac{N}{2}-1} \hat{h}(k_x, k_y, k_z, t) e^{ik_x x_j + ik_y y_j + ik_z z_j}, \quad 0 \le j \le N - 1. \quad (14)$$

To sum up, the steps of solving fractional partial differential equations by the Fourier spectral method are as follows:

$$
\begin{array}{cccccccccc}
u_{j-N/2} & \cdots & u_{j-2} & u_{j-1} & u_j & u_{j+1} & u_{j+2} & \cdots & u_{j+N/2-1} & u(x,y,z,t) \\
 & & & & \Uparrow IDFT & & & & & \\
\bullet & \cdots & \bullet & \bullet & \bullet & \bullet & \bullet & \cdots & \bullet & \hat{u}(K_\alpha, t) \\
\uparrow & & \uparrow & \uparrow & \uparrow & \uparrow & \uparrow & & \uparrow & \\
\bullet & \cdots & \bullet & \bullet & \bullet & \bullet & \bullet & \cdots & \bullet & \\
 & & & & ODEs & & & & & \leftarrow RKM \\
\bullet & \cdots & \bullet & \bullet & \bullet & \bullet & \bullet & \cdots & \bullet & \\
\uparrow & & \uparrow & \uparrow & \uparrow & \uparrow & \uparrow & & \uparrow & \\
\hat{u}_{m-N} & \cdots & \hat{u}_{m-2} & \hat{u}_{m-1} & \hat{u}_m & \hat{u}_{m+1} & \hat{u}_{m+2} & \cdots & \uparrow & \hat{u}(K_\alpha, t_0) \\
 & & & & \Uparrow DFT & & & & & \\
u_{j-N/2} & \cdots & u_{j-2} & u_{j-1} & u_j & u_{j+1} & u_{j+2} & \cdots & u_{j+N/2-1} & u(x,y,z,t_0)
\end{array}
$$
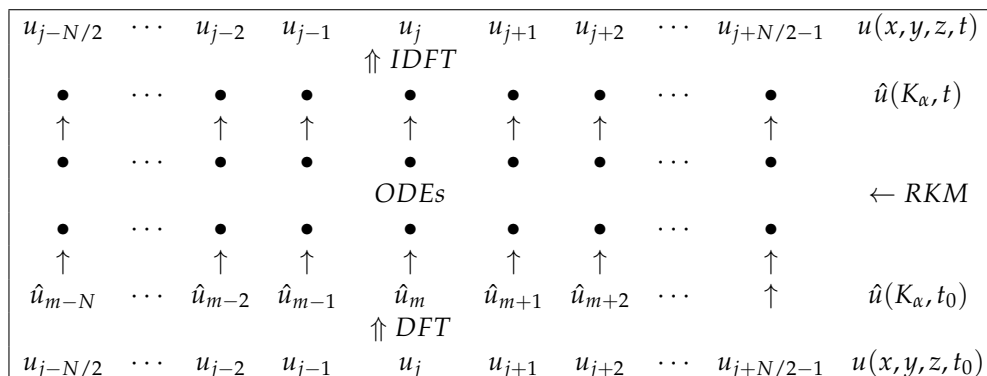
3. Simulation Results

Figure 1 shows the logarithm of the absolute error at $x = 0.5$. The absolute error values at $t = 0.15$ are shown in Figure 2. In this section, we use the present method to numerically solve the space fractional 2D and 3D coupled FitzHugh–Nagumo models and space fractional coupled Gray–Scott models, the numerical simulation results are shown in Figures 3–18. All computations of simulation results are performed by the MatlabR2017b software.

Experiment 1. *By comparing with some effective methods in the literature, the accuracy and effectiveness of the numerical method in this paper are illustrated. We consider the following 1D FitzHugh–Nagumo model [43,44].*

$$
\frac{\partial u}{\partial t} = u_{xx} + u(1-u)(u-\mu), \tag{15}
$$

Table 1 shows the absolute errors by the present method, and those in Refs. [43,44], at different x values. Table 2 shows the error norms L_2 and L_∞ by the present method and the methods of Ref. [44] at different τ values, which shows that our numerical method has higher precision than other methods.

Where the error norms, L_2 and L_∞ are used to determine the accuracy of the method: $L_2 = \sqrt{\frac{1}{N} \sum_{j=1}^{N} [u(x_j, t) - u^*(x_j, t)]^2}$, $L_\infty = \max_{1 \le j \le N} | u(x_j, t) - u^*(x_j, t) |$, where $u(x_j, t)$ and $u^*(x_j, t)$ are the numerical solution and the exact solution.

Table 1. The absolute errors of $u(x,t)$ at $t = 0.04$, $\tau = 5.00e - 3$, and $\mu = 0.5$.

x	ExpFDM [43]	Ref. [44]	Present Method
0.2	3×10^{-6}	2×10^{-7}	1.67×10^{-10}
0.4	1×10^{-5}	5×10^{-7}	1.69×10^{-10}
0.6	2×10^{-5}	7×10^{-7}	1.72×10^{-10}
0.8	4×10^{-5}	6×10^{-7}	1.77×10^{-10}

Table 2. The error norms L_2 and L_∞ of $u(x,t)$ at different values of τ and $\mu = 0.75$, for example, 1.

$\tau = 0.001$	t	$t = 0.01$	$t = 1$	$t = 10$
L_2	Present method	2.17×10^{-9}	2.08×10^{-10}	3.66×10^{-9}
	[44] method	1×10^{-7}	1×10^{-6}	2×10^{-7}
L_∞	Present method	2.07×10^{-9}	2×10^{-10}	5.41×10^{-9}
	[44] method	2×10^{-7}	1×10^{-6}	2×10^{-7}
$\tau = 0.0001$	t	$t = 0.01$	$t = 1$	$t = 10$
L_2	Present method	2.17×10^{-9}	1.51×10^{-9}	3.36×10^{-9}
	[44] method	1×10^{-7}	6×10^{-7}	2×10^{-7}
L_∞	Present method	2.07×10^{-9}	1.47×10^{-9}	5.42×10^{-9}
	[44] method	2×10^{-7}	9×10^{-7}	3×10^{-7}
$\tau = 0.00001$	t	$t = 0.01$	$t = 1$	$t = 10$
L_2	Present method	2.17×10^{-9}	4.08×10^{-9}	3.37×10^{-9}
	[44] method	1×10^{-7}	6×10^{-7}	2×10^{-7}
L_∞	Present method	2.07×10^{-9}	3.90×10^{-9}	5.49×10^{-9}
	[44] method	2×10^{-7}	9×10^{-7}	3×10^{-7}
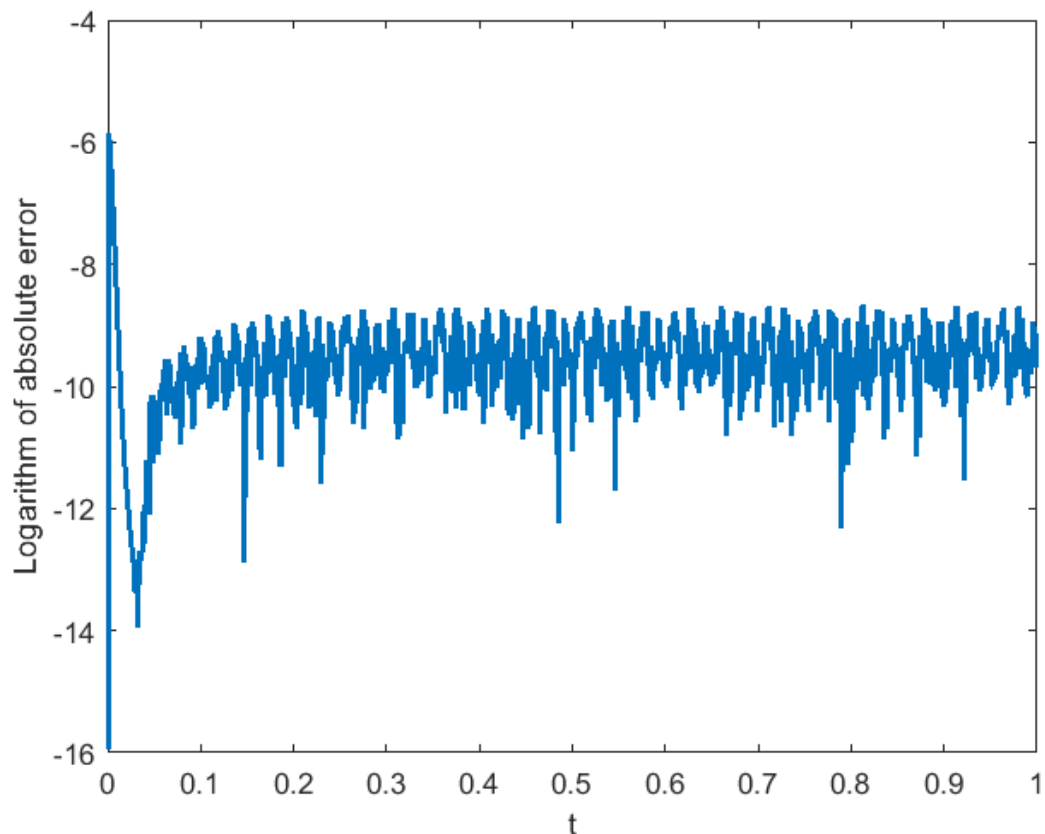
**Figure 1.** Logarithm of absolute error of $u(x,t)$ at $x = 0.5$ for Experiment 1.
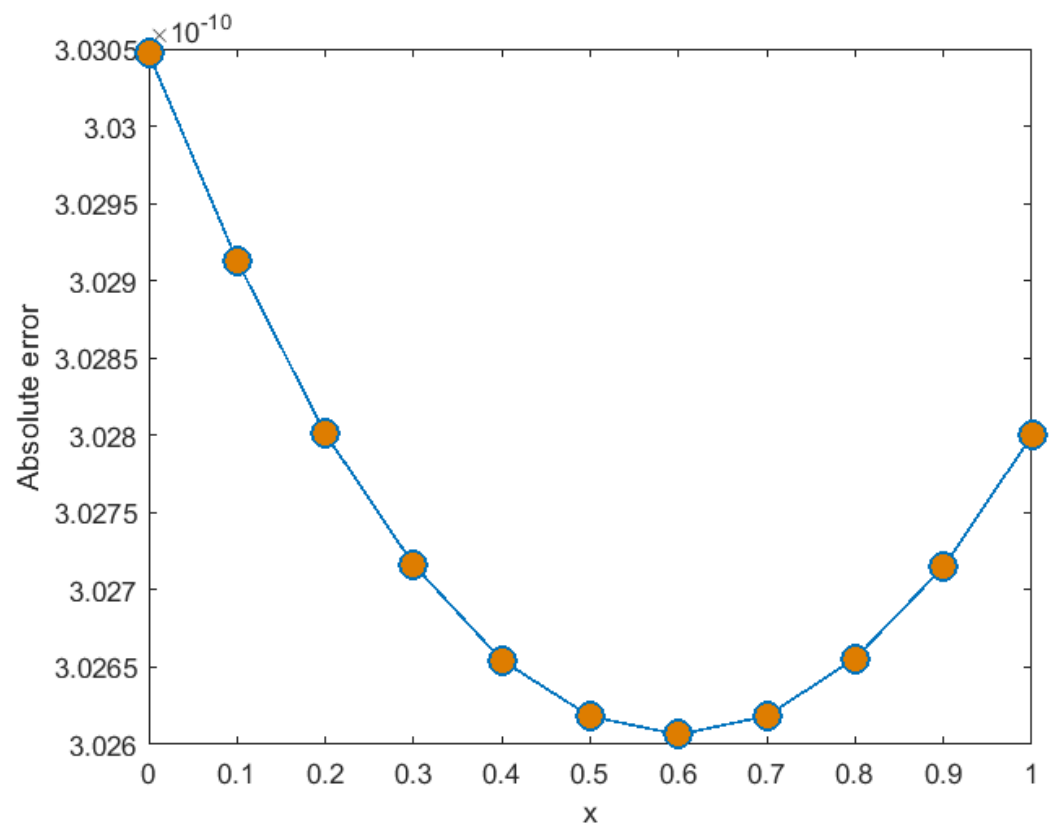
Figure 2. Absolute error of $v(x, t)$ at $t = 0.15$ for Experiment 1.

Experiment 2. *In the simulation experiment, we set $v = v(x, y, t)$ or $v = v(x, y, z, t)$ with similar expressions for u in two and three dimensions. In two dimensions, we experiment (1) on a square domain size $[-2.5, 2.5] \times [-2.5, 2.5]$ with boundary conditions. We experiment (1) on diffusion coefficients in the space given as $K_u = 1 \times 10^{-4}$, and parameter $\varepsilon = 0.01, \mu = 0.1, \beta = 0.5, N = 512, L = 5$. The initial conditions have the following form:*

$$u(x, y, 0) = \begin{cases} 1, & (x, y) \in [-0.63, 0.62] \times [0.62, 1.24] \cup [-0.63, 1.26], \\ 0, elsewhere. \end{cases} \tag{16}$$

$$v(x, y, 0) = \begin{cases} 0.1, & (x, y) \in [-1.88, -0.63] \cup [0.62, 2.5] \times [-1.26, 2.5], \\ 0, elsewhere. \end{cases} \tag{17}$$

The spatio-temporal patterns in Figure 3 are obtained at different times with the same α value. The patterns in Figures 4–6 are obtained at the same time and different α values. When noise intensity $K_u = 1 \times 10^{-4}$, spiral wave can be sustained for a long time (see Figure 3). With the increment of fractional derivative α, the system is driven into the excitable states where the stable spatio-temporal waves can be sustained for a long time (see Figures 4–6). We can find that the width of the excitation wavefront and the wavelength of the system are markedly reduced with the reduction of order with the domain being able to accommodate a larger number of wavefronts for a smaller order. For the excited wavefront with approximately the same width, the wavelength is larger due to the long-tailed mechanisms of the fractional Laplacian operator in the supper-diffusion case. These results are consistent with the theoretical analysis and numerical simulation of other scholars [45].

The spatio-temporal patterns in Figures 7–9 are obtained at different times and α values with the noise intensity $K_u = 2.5 \times 10^{-5}$, the initial conditions have the following form:

$$u(x,y,0) = \begin{cases} u(3*N/8:5*N/8,5*N/8:6*N/8) = 1, \\ u(3*N/8:5*N/8,2*N/8:3*N/8) = 1, \\ 0, elsewhere. \end{cases} \tag{18}$$

$$v(x,y,0) = \begin{cases} v(5*N/8:N,N/4:N) = 0.1, \\ v(1*N/8:3*N/8,N/4:N) = 0.1, \\ \\ 0, elsewhere. \end{cases} \tag{19}$$

In three dimensions, we experiment (1) on the domain size $[-2.5, 2.5] \times [-2.5, 2.5] \times [-2.5, 2.5]$ with boundary conditions. We set different values of α and t, the stable patterns in Figures 10–13 are obtained with $K_u = 1 \times 10^{-4}$, $\varepsilon = 0.0001$, $\mu = 0.01$, $\beta = 0.5$, $L = 5, N = 512$. The initial conditions are: $u(3N/8 : 5N/8, 5N/8 : 6N/8, 5N/8 : 6N/8, 0) = u(3N/8 : 5N/8, 2N/8 : 3N/8, 2N/8 : 3N/8, 0) = 1$, elsewhere $u = 0$. $v(5N/8 : N, N/4 : N, N/4 : N, 0) = 0.1$, elsewhere, $v = 0$. We showed some patterns in Figures 10–13 of fractional-in-space nonlinear coupled FitzHugh–Nagumo models for the first time. Some patterns in Figures 10–13 are different from any previously obtained in numerical studies.


(**a**) $t = 400$ (**b**) $t = 600$ (**c**) $t = 1000$ (**d**) $t = 2000$ (**e**) $t = 3000$
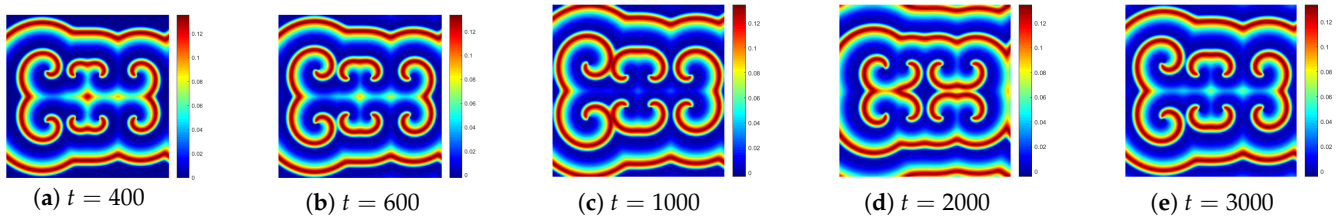
Figure 3. The stable spatio-temporal waves of v at $\alpha = 2$ and different times for Experiment 2.

(**a**) $\alpha = 1.6$ (**b**) $\alpha = 1.7$ (**c**) $\alpha = 1.8$ (**d**) $\alpha = 1.90$
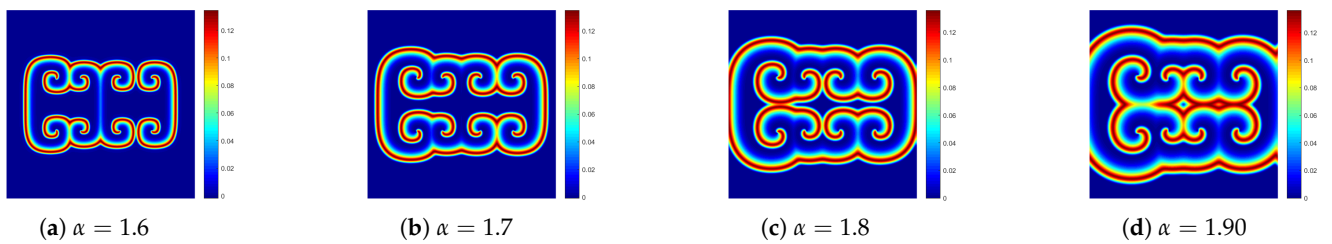
Figure 4. The stable spatio-temporal waves of v at $t = 400$ for Experiment 2.

(**a**) $\alpha = 1.5$ (**b**) $\alpha = 1.6$ (**c**) $\alpha = 1.7$ (**d**) $\alpha = 1.8$ (**e**) $\alpha = 1.9$
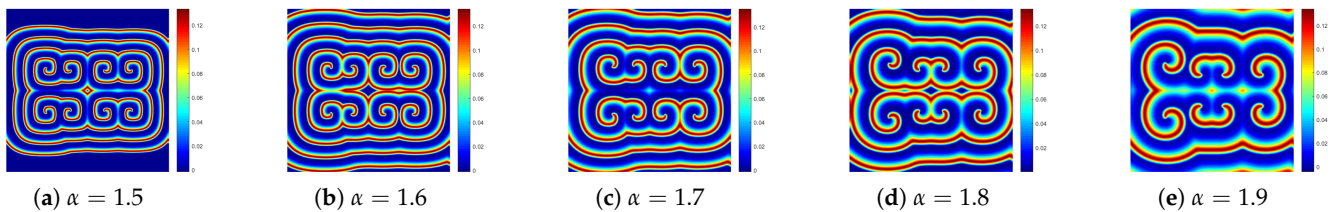
Figure 5. The stable spatio-temporal waves of v at $t = 1000$ and different α for Experiment 2.

(**a**) $\alpha = 1.5$ (**b**) $\alpha = 1.6$ (**c**) $\alpha = 1.7$ (**d**) $\alpha = 1.8$ (**e**) $\alpha = 1.9$
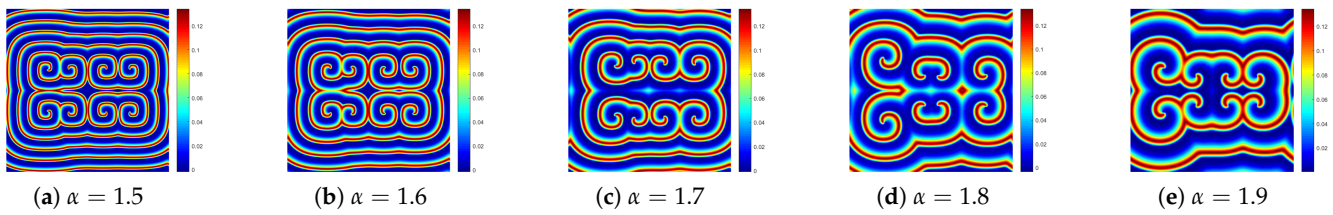
Figure 6. The stable spatio-temporal waves of v at $t = 2000$ and different α for Experiment 2.

(**a**) $t = 400$ (**b**) $t = 600$ (**c**) $t = 1000$ (**d**) $t = 2000$
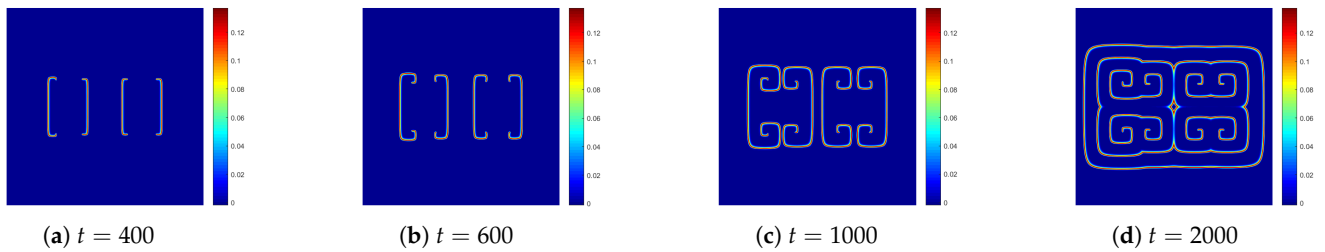
Figure 7. The stable spatio-temporal waves of v at $\alpha = 1.5$ and different times for Experiment 2.

(**a**) $t = 400$ (**b**) $t = 600$ (**c**) $t = 1000$ (**d**) $t = 2000$
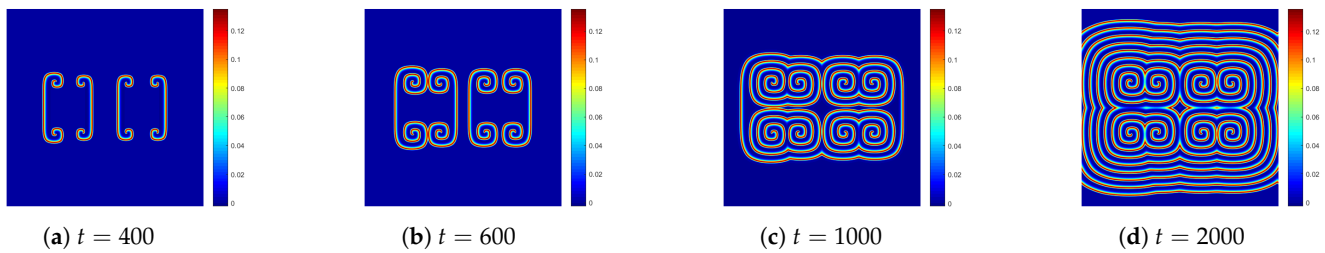
Figure 8. The stable spatio-temporal waves of v at $\alpha = 1.6$ and different times for Experiment 2.

(**a**) $t = 400$ (**b**) $t = 600$ (**c**) $t = 1000$ (**d**) $t = 2000$
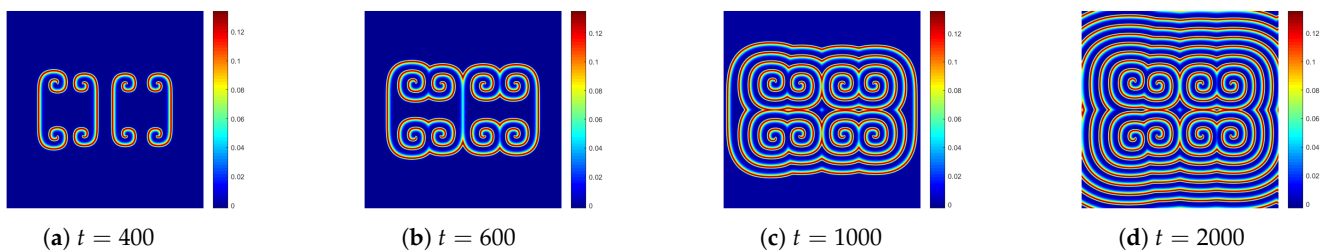
Figure 9. The stable spatio-temporal waves of v at $\alpha = 1.7$ and different times for Experiment 2.

(**a**) $t = 500$ (**b**) $t = 1000$ (**c**) $t = 2000$ (**d**) $t = 3000$
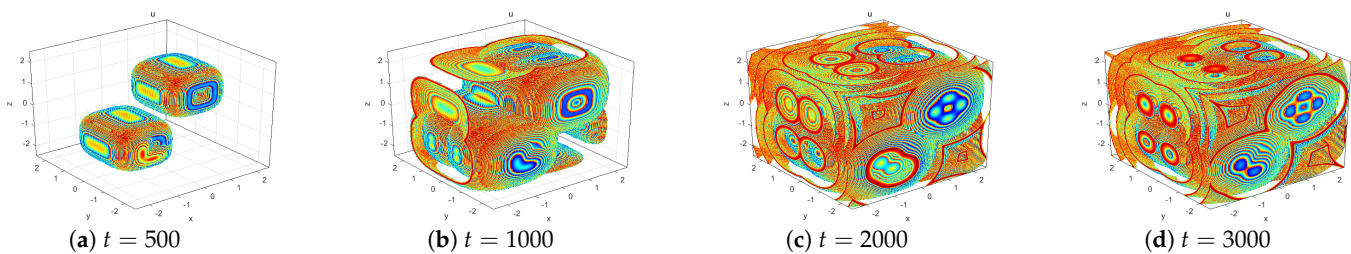
Figure 10. The patterns of u at $K_u = 1 \times 10^{-4}$, $\varepsilon = 0.0001$, $\mu = 0.01$, $\beta = 0.5$, $N = 512$, and $\alpha = 1.8$.

(a) $t = 500$ **(b)** $t = 1000$ **(c)** $t = 2000$ **(d)** $t = 3000$
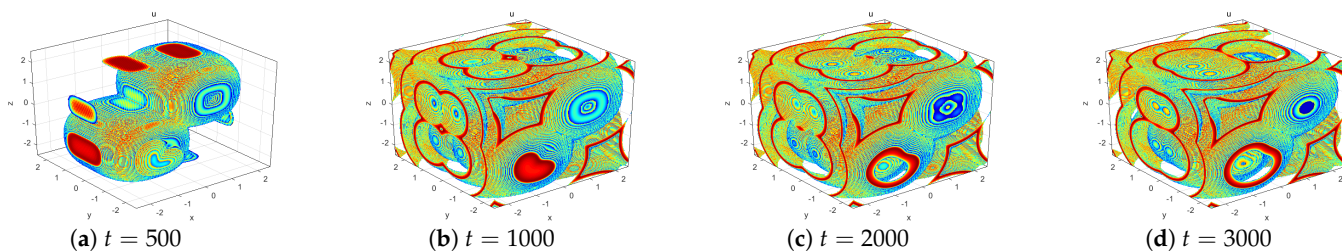
Figure 11. The patterns of u at $K_u = 1 \times 10^{-4}$, $\varepsilon = 0.0001$, $\mu = 0.01$, $\beta = 0.5$, $N = 512$, and $\alpha = 2$.

(a) $t = 1000$ **(b)** $t = 2000$ **(c)** $t = 3000$
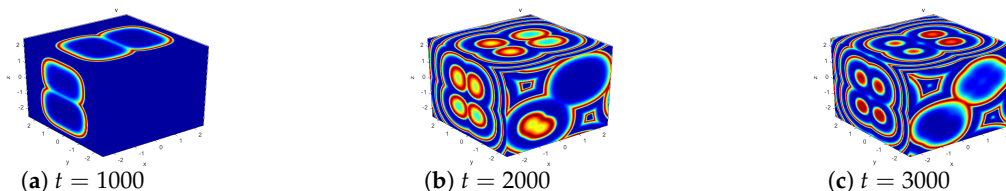
Figure 12. The patterns of v at $K_u = 1 \times 10^{-4}$, $\varepsilon = 0.0001$, $\mu = 0.01$, $\beta = 0.5$, $N = 512$, and $\alpha = 1.8$.


**(a)** $t = 1000$ **(b)** $t = 2000$ **(c)** $t = 3000$
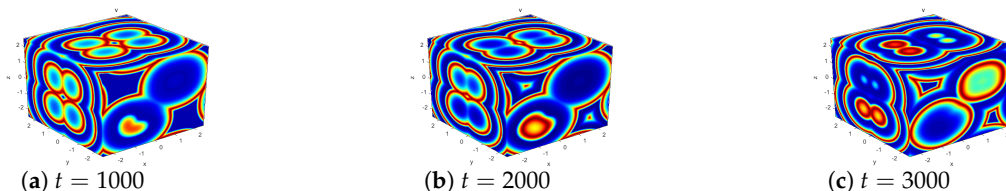
Figure 13. The patterns of v at $K_u = 1 \times 10^{-4}$, $\varepsilon = 0.0001$, $\mu = 0.01$, $\beta = 0.5$, $N = 512$, and $\alpha = 2$.

Experiment 3. *Numerical simulation provides us with a universal approach to physical insight into fractional reaction-diffusion model. Next, we simulate the following space fractional coupled Gray–Scott model [37–40],*

$$\begin{cases} \dfrac{\partial u}{\partial t} = -K_u(-\Delta^{\frac{\alpha}{2}})u - uv^2 + F(1-u), \\ \dfrac{\partial v}{\partial t} = -K_v(-\Delta^{\frac{\beta}{2}})v + uv^2 - (F+k)v. \end{cases} \tag{20}$$

In the simulation Experiment, we set $v = v(x, y, t)$ or $v = v(x, y, z, t)$ with similar expressions for u in two and three dimensions. In two dimensions, we experiment (20) on a square domain size $[-1, 1] \times [-1, 1]$ with boundary conditions. A 64×64 mesh point area located symmetrically about the centre of the grid was perturbed to $(u, v) = (\frac{1}{2}, \frac{1}{4})$, and the entire model was placed in the state $(u, v) = (1, 0)$. The patterns in Figure 14 were obtained with the diffusion coefficients in space given as $D_u = 2 \times 10^{-5}$, $D_v = 1 \times 10^{-5}$, $F = 0.025$, $k = 0.055$, $L = 2$, $N = 128$, and the time step is $\tau = 0.01$. The patterns in Figure 15 were obtained with the diffusion coefficients in space given as $D_u = 2 \times 10^{-5}$, $D_v = 1 \times 10^{-5}$, $\tau = 0.01$. $F = 0.037$, $k = 0.058$, and the time step is $\tau = 0.01$.

In three dimensions, we experiment (20) on the domain size $[-1, 1] \times [-1, 1] \times [-1, 1]$ with boundary conditions. A $32 \times 32 \times 32$ mesh point area located symmetrically about the centre of the grid was perturbed to $(u, v) = (\frac{1}{2}, \frac{1}{4})$, and the entire model was placed in the state $(u, v) = (1, 0)$. We show some patterns in Figures 16–18 of the space fractional 3D coupled Gray–Scott model are different from any previously obtained in numerical studies. The patterns in Figure 16 were obtained with the diffusion coefficients in space given as $K_u = 2 \times 10^{-5}$, $K_v = 1 \times 10^{-5}$, $F = 0.02$, $k = 0.055$, $N = 128$, and $\alpha = \beta = 1.8$. The patterns in Figure 17 were obtained with the diffusion coefficients in space given as $K_u = 2 \times 10^{-5}$, $K_v = 1 \times 10^{-5}$, $F = 0.015$, $k = 0.045$, and $\alpha = \beta = 1.9$. The patterns in Figure 18 were obtained with the diffusion coefficients in space given as $K_u = 2 \times 10^{-5}$, $K_v = 1 \times 10^{-5}$, $F = 0.02$, $k = 0.055$, $N = 128$, and $\alpha = \beta = 1.9$. The time step was $\tau = 0.01$.
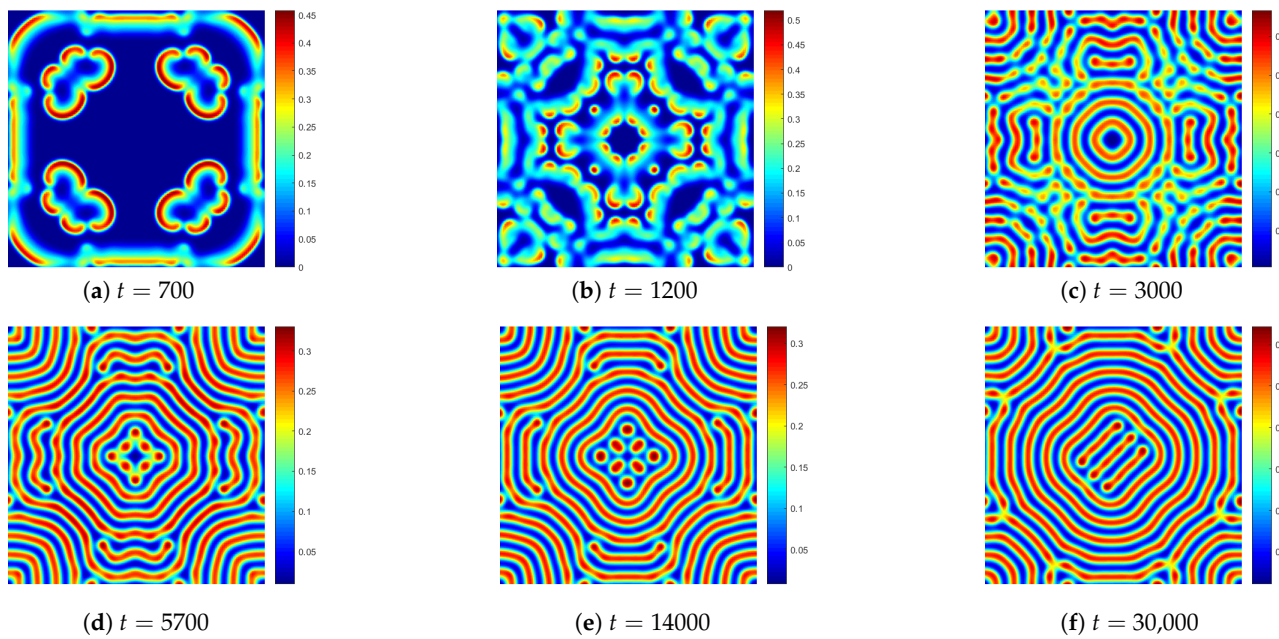
Figure 14. The patterns of u at $\alpha = \beta = 1.9$ for Experiment 3 with $D_u = 2 \times 10^{-5}$, $D_v = 1 \times 10^{-5}$, $F = 0.025$, $k = 0.055$, $L = 2$, $N = 128$.
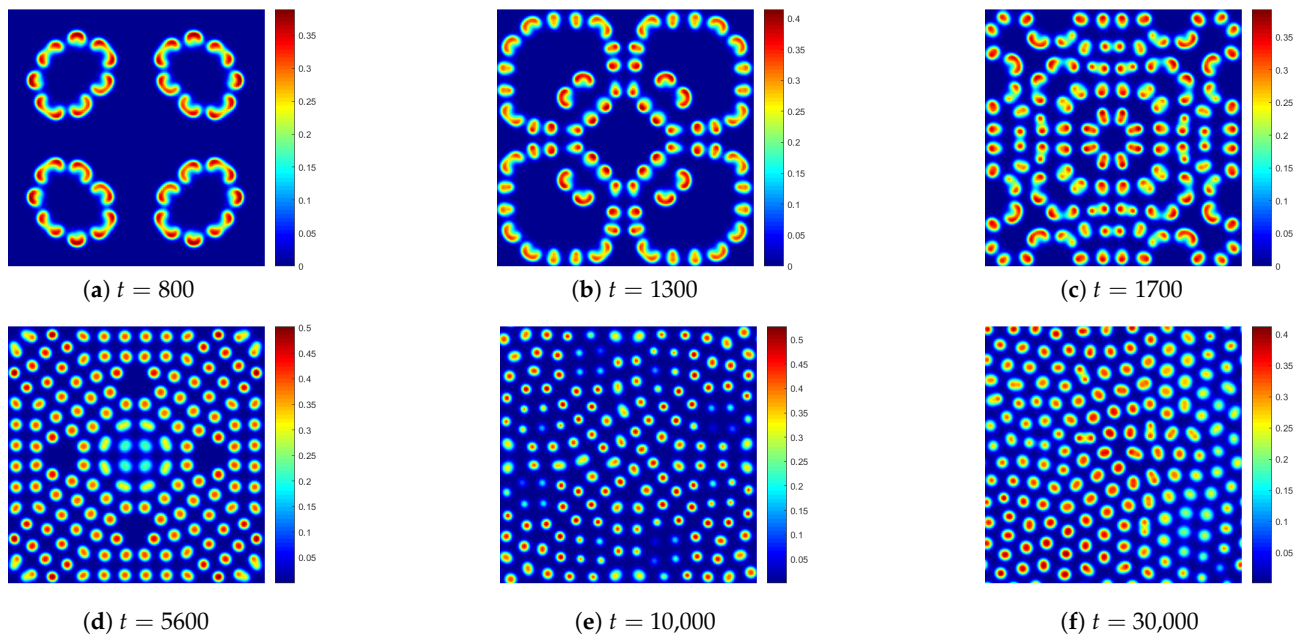

Figure 15. The patterns of u at $\alpha = \beta = 1.9$ for Experiment 3 with $D_u = 2 \times 10^{-5}$, $D_v = 1 \times 10^{-5}$, $\tau = 0.01$. $F = 0.037$, $k = 0.058$.
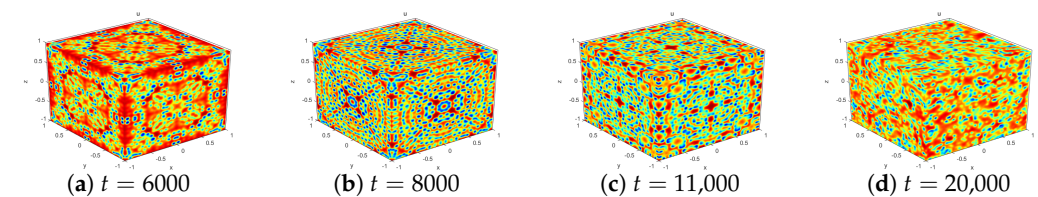
Figure 16. The patterns of u at $K_u = 2 \times 10^{-5}$, $K_v = 1 \times 10^{-5}$, $F = 0.02$, $k = 0.055$, $N = 128$, and $\alpha = \beta = 1.8$ for Experiment 3.

| (a) $t = 5000$ | (b) $t = 10,000$ | (c) $t = 15,000$ | (d) $t = 20,000$ |
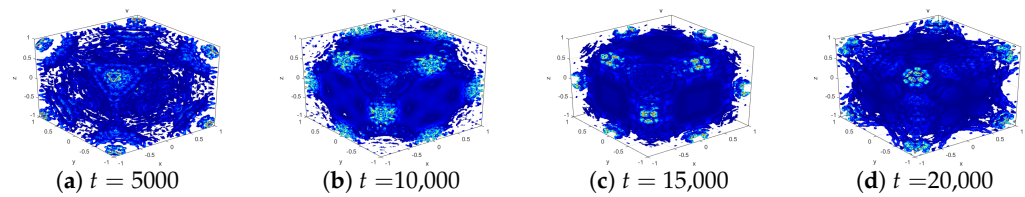
Figure 17. The patterns of v at $K_u = 2 \times 10^{-5}$, $K_v = 1 \times 10^{-5}$, $F = 0.015$, $k = 0.045$, and $\alpha = \beta = 1.9$ for Experiment 3.

| (a) $t = 6000$ | (b) $t = 8000$ | (c) $t = 11,000$ | (d) $t = 20,000$ |
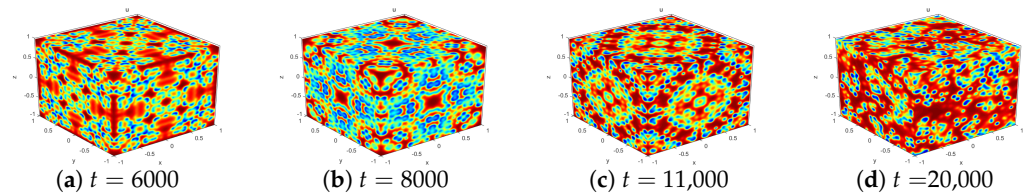
Figure 18. The patterns of u at $K_u = 2 \times 10^{-5}$, $K_v = 1 \times 10^{-5}$, $F = 0.02$, $k = 0.055$, $N = 128$, and $\alpha = \beta = 1.9$ for Experiment 3.

4. Conclusions

In this paper, the Fourier spectral method is used to solve the fractional-in-space nonlinear coupled FitzHugh–Nagumo model. It is found that the results of numerical experiments are consistent with the theoretical results of other scholars, which verifies the accuracy of the method. We show that 3D stable spatio-temporal spiral patterns can be sustained for a long time; these spiral waves are different from any previously obtained in numerical studies. The numerical results in Experiment 1 show that the present method has strong competitiveness and reliability. In Experiment 3, we simulate 2D and 3D fractional-in-space nonlinear coupled Gray–Scott models. The reliability and efficiency are verified by numerical experiments. The present method provides us with a universal approach and insight into the fractional reaction-diffusion model. The results show that the fractional FitzHugh–Nagumo model and Gray–Scott model can describe the pattern behavior well, and that the fractional reaction-diffusion model has unique properties that the integer model does not have.

Author Contributions: Conceptualization, Y.W. and X.L.; data curation and formal analysis, Y.W.; funding acquisition, C.H.; methodology, X.L.; software, C.H. and X.L.; validation, Y.W. and X.L.; writing—original draft and writing—review and editing, Y.W., X.L. and C.H. All authors have read and agreed to the published version of the manuscript.

Data Availability Statement: The data used to support the findings of this study are available from the corresponding author upon request.

Conflicts of Interest: The authors declare that there is no conflict of interest regarding the publication of this article.

References

1. Li, Y.; Chen, Y.Q.; Podlubny, I. Mittag-Leffler stability of fractional order nonlinear dynamic systems. *Automatica* **2009**, *45*, 1965–1969. [CrossRef]
2. Tan, W.; Xu, M. Plane surface suddenly set in motion in a viscoelastic fluid with fractional Maxwell model. *Acta Mech. Sin.* **2002**, *18*, 342–349.
3. Scott-Blair, G.W. The role of psychophysics in rheology. *J. Colloid Sci.* **1947**, *2*, 21–32. [CrossRef]
4. Ding, C.; Cao, J.; Chen, Y.Q. Fractional-order model and experimental verification for broadband hysteresis in piezoelectric actuators. *Nonlinear Dyn.* **2019**, *98*, 3143–3153. [CrossRef]
5. Sokolov, I.M.; Klafter, J.; Blumen, A. Fractional kinetics. *Phys. Today* **2002**, *55*, 48–54. [CrossRef]

6.   Gerasimov, A.N. A generalization of linear laws of deformation and its application to inner friction problems. *Prikl. Math. Mekh.* **1948**, *12*, 251–259.

7.   Schneider, W.R.; Wyss, W. Fractional diffusion and wave equations. *J. Math. Phys.* **1989**, *30*, 134–144. [CrossRef]

8.   Metzler, R.; Glockle, W.G.; Nonnenmacher, T.F. Fractional model equation for anomalous diffusion. *Phys. A Stat. Mech. Its Appl.* **1994**, *211*, 13–24. [CrossRef]

9.   Jiang, X.; Xu, M.; Qi, H. The fractional diffusion model with an absorption term and modified Fick's law for non-local transport processes. *Nonlinear Anal. Real World Appl.* **2010**, *11*, 262–269. [CrossRef]

10.   Adomian, G. *Solving Frontier Problems in Physics: The Decomposition Method*; Kluwer Academic: Boston, MA, USA, 1994.

11.   Daftardar-Gejji, V.; Jafari, H. An iterative method for solving nonlinear functional equations differential equations. *J. Math. Anal. Appl.* **2006**, *316*, 321–354. [CrossRef]

12.   He, J.H.; El-Dib, Y.O.; Mady, A.A. Homotopy perturbation method for the fractal toda oscillator. *Fractal Fraction* **2021**, *5*, 93. [CrossRef]

13.   Zhang, Y.; Cao, J.; Bu, W.; Xiao, A. A fast finite difference/finite element method for the two-dimensional distributed-order time-space fractional reaction-diffusion equation. *Int. J. Model. Simul. Sci. Comput.* **2020**, *11*, 2050016 . [CrossRef]

14.   Daftardar-Gejji, V.; Sukale, Y.; Bhalekar, S. A new predictor-corrector method for fractional differential equations. *Appl. Math. Comput.* **2014**, *244*, 158–182. [CrossRef]

15.   Jhinga, A.; Daftardar-Gejji, V. A new finite difference predictor-corrector method for fractional differential equations. *Appl. Math. Comput.* **2018**, *336*, 418–432. [CrossRef]

16.   Wang, Y.L.; Jia, L.N.; Zhang, H.L. Numerical solution for a class of space-time fractional equation in reproducing. *Int. J. Comput. Math.* **2019**, *96*, 2100–2111. [CrossRef]

17.   Dai, D.D.; Ban, T.T.; Wang, Y.L.; Zhang, W. The piecewise reproducing kernel method for the time variable fractional order advection-reaction-diffusion equations. *Therm. Sci.* **2021**, *25*, 1261–1268. [CrossRef]

18.   Podlubny, I. Matrix approach to discrete fractional calculus. *Fract. Calc. Appl. Anal.* **2000**, *3*, 359–386.

19.   Wang, J.J.; Xiao, A.G. Conservative Fourier spectral method and numerical investigation of space fractional Klein-Gordon-Schrödinger equations. *Appl. Math. Comput.* **2019**, *350*, 348–365. [CrossRef]

20.   Zhao, X.; Liu, B.; Zhang, P.; Zhang, W.; Liu, F. Fourier spectral method for the modified Swift-Hohenberg equation. *Adv. Differ. Equ.* **2013**, *2013*, 156. [CrossRef]

21.   Bueno-Orovio, A.; Kay, D.; Burrage, K. Fourier spectral methods for fractional-in-space reaction-diffusion equations. *Bit Numer. Math.* **2014**, *54*, 937–954. [CrossRef]

22.   Pelz, R.B. Fourier spectral method on ensemble architectures. *Comput. Methods Appl. Mech. Eng.* **1991**, *89*, 529–542. [CrossRef]

23.   Xue, D.Y. *Fractional Calculus and Fractional-Order Control*; Science Press: Beijing, China, 2018.

24.   Owolabi, K.M.; Atangana, A. *Numerical Methods for Fractional Differentiation*; Springer: Singapore, 2019.

25.   Atangana, A.; Alqahtani, R.T. New numerical method and application to Keller-Segel model with fractional order derivative. *Chaos Solitons Fractals* **2018**, *116*, 14–21. [CrossRef]

26.   Yang, X.J.; Baleanu, D.; Srivastava, H.M. Local fractional similarity solution for the diffusion equation defined on Cantor sets. *Appl. Math. Lett.* **2015**, *47*, 54–60. [CrossRef]

27.   Podlubny, I. *Fractional Differential Equations: An Introduction to Fractional Derivatives, Fractional Differential Equations, to Methods of Their Solution and Some of Their Applications*; Academic Press: New York, NY, USA, 1998.

28.   Podlubny, I. Geometric and physical interpretations of fractional integration and differentiation. *Fract. Calc. Appl. Anal.* **2001**, *5*, 230–237.

29.   Yang, X.J. *General Fractional Derivatives: Theory, Methods and Applications*; CRC Press: New York, NY, USA, 2019.

30.   Han, C.; Wang, Y.L.; Li, Z.Y. Numerical solutions of space fractional variable-coefficient KdV-modified KdV equation by Fourier spectral method. *Fractals* **2021**, *29*, 2150246. [CrossRef]

31.   Han, C.; Wang, Y.L.; Li, Z.Y. A high-precision numerical approach to solving space fractional Gray-Scott model. *Appl. Math. Lett.* **2022**, *125*, 107759. [CrossRef]

32.   Fitzhugh, R. Mathematical models of threshold phenomena in the nerve membrane. *Bull. Math. Biophys.* **1995**, *17*, 257–269. [CrossRef]

33.   Nagumo, J.; Arimoto, S.; Yoshizawa, S. An active pulse transmission line simulating nerve axon. *Proc. IRE* **1962**, *50*, 2061–2070. [CrossRef]

34.   Magin, R.L.; Abdullah, O.; Baleanu, D.; Zhou, X.J. Anomalous diffusion expressed through fractional order differential operators in the Bloch-Torrey equation. *J. Magn. Reson.* **2008**, *190*, 255–270. [CrossRef]

35.   Meerschaert, M.M.; Mortensen, J.; Wheatcraft, S.W. Fractional vector calculus for fractional advection-dispersion. *Phys. A Stat. Mech. Its Appl.* **2006**, *367*, 181–190. [CrossRef]

36.   Liu, F.W.; Zhuang, P.H.; Turner, I.; Anh, V.; Burrage, K. A semi-alternating direction method for a 2-D fractional FitzHugh-Nagumo monodomain model on an approximate irregular domain. *J. Comput. Phys.* **2015**, *293*, 252–263. [CrossRef]

37.   Lee, G.H. A second-order operator splitting Fourier spectral method for fractional-in-space reaction-diffusion equations. *J. Comput. Appl. Math.* **2018**, *33*, 395–403. [CrossRef]

38.   Wang, T.T.; Song, F.Y.; Wang, H.; Karniadakis, G.E. Fractional Gray-Scott model: Well-posedness, discretization, and simulations. *Comput. Methods Appl. Mech. Eng.* **2019**, *347*, 1030–1049. [CrossRef]

39. Liu, Y.; Fan, E.Y.; Yin, B.L.; Li, H.; Wang, J. TT-M finite element algorithm for a two-dimensional space fractional Gray-Scott model. *Comput. Math. Appl.* **2020**, *80*, 1793–1809. [CrossRef]
40. Zhang, H.; Jiang, X.Y.; Zeng, F.H.; Karniadakis, G.E. A stabilized semi-implicit Fourier spectral method for nonlinear space-fractional reaction-diffusion equations. *J. Comput. Phys.* **2019**, *405*, 109141. [CrossRef]
41. Kilbas, A.A.; Srivastava, H.M.; Trujillo, J.J. *Theory and Applications of Fractional Differential Equations*; Elsevier: Amsterdam, The Netherlands, 2006.
42. Atanackovic, T.M.; Pilipovic, S.; Stankovic, B.; Zorica, D. *Fractional Calculus with Applications in Maechanics*; John Willey Sons Inc.: Hoboken, NJ, USA, 2014.
43. Ruiz-Ramirez, J.; Macias-Diaz, J.E. A finite-difference scheme to approximate non-negative and bounded solutions of a FitzHugh-Nagumo equation. *Int. J. Comput. Math.* **2011**, *88*, 3186–3201. [CrossRef]
44. INan, B.; Ali, K.K.; Saha, A.; Ak, T. Analytical and numerical solutions of the Fitzhugh-Nagumo equation and their multistability behavior. *Numer. Methods Partial Differ. Equ.* **2021**, *37*, 7–23. [CrossRef]
45. Engler, H. On the speed of spread for fractional reaction-diffusion equations. *Int. J. Differ. Equ.* **2010**, *315*, 315–421. [CrossRef]